

Comprehensive Analysis for Electric Field and Potential for Polymeric and Ceramic Insulators

Mohamad Saleh Sanjari Nia^{*}, Mohammad Altimania, Pourya Shamsi, Mehdi Ferdowsi

Department of Electrical Engineering, Missouri University of Science and Technology, Rolla, MO 65409 USA

^{*}Corresponding author: mswvq@mst.edu

Received December 04, 2019; Revised January 06, 2020; Accepted January 11, 2020

Abstract The principal object of this paper is to provide a comprehensive approach for parallel processing of potential and electric field calculations. The approach investigated under dry and wet conditions for two types of insulators, the ceramic cap and pin and the polymeric, in three different high voltages: 230 kV, 400 kV, and 765 kV account for the two design factors: towers and bundled conductors. Moreover, corona is an important phenomenon associated with all transmission lines that causes the surrounding air molecules to ionize, or undergo a slight localized change of electric charge. As such, the effects of the corona rings on the insulators considering potential and electric field distribution are other objects of this paper. Decisively, this requires accurate and efficient modeling of the proposed insulators on the tower conductors of the transmission lines which is derived by a detailed localized potential and electric field distribution approach that combines the different aspects of the transmission high voltages. The corona rings' optimization for six individual insulators is another object of this study.

Keywords: ceramic insulators, dry and wet conditions, optimization, polymeric insulators, electric field and potential distribution

Cite This Article: Mohamad Saleh Sanjari Nia, Mohammad Altimania, Pourya Shamsi, and Mehdi Ferdowsi, "Comprehensive Analysis for Electric Field and Potential for Polymeric and Ceramic Insulators." *American Journal of Electrical and Electronic Engineering*, vol. 8, no. 1 (2020): 26-34. doi: 10.12691/ajeec-8-1-4.

1. Introduction

Computation of the electric field and potential distribution along insulators play an important role in designing and manufacturing electrical equipment and transmission lines. The Polymeric and the ceramic insulators each have special features in terms of the electric field and the potential distribution, which can cause corona and flashover problems [1-4]. Adjusting corona rings and adding bundled conductors can prevent flashover and decrease corona under dry and wet circumstances by considering the system voltage, which can enhance reliability, productivity, and economic efficiency [5-23].

Features like reduced weight, ease of installation, cost reduction, and better performance against environmental pollution are benefits of polymeric insulators [24,25]. However, they might erode when subjected to sustained electrical discharge. In addition, the distribution of their internal electric field is more nonlinear than ceramic insulators, which can lead to corona and increase various failure modes [25,26].

One of the significant design factors in transmission lines is corona discharge, due to the losses that the discharge imposes on the system along with radio interferences [27]. To control this phenomenon, corona rings are widely used in high voltage transmission lines.

At 230 kV and higher, though some cases under 230 kV, adjusting the ring size is effectively deconcentrates the electric field and decreases the radio interference and loss [24,25]. In High Voltage (HV) and Extra high Voltage (EHV) applications, transmission lines use bundled conductors to prevent high electric field concentrations and reduce current losses in conductors [25]. Bundling conductors and its effects on the electric field and voltage distribution in insulators depend on the number of bundles, which is used to decrease corona and radio interferences.

There are two main approaches to finding the distribution of the electric field and potential along insulators at various voltage ratings. The first method is using laboratory equipment and instruments to extract empirical results [28]. This method is expensive and time consuming. A better method is to use a numerical method using computers [28,29]. Several methods are used to calculate the electric field and voltage in special geometries [29-32]. Among them is the finite element method (FEM), which is very popular for computing complex geometries and nonlinear properties of materials and is very powerful.

In [9], by considering the electric field distribution in 380 kV V-string ceramic insulators, the corona rings were optimized by considering different points of views, such as economic, flashover, etc. In spite of considering the effects of towers and bundled conductors in [9], the results are only acceptable for one specific voltage and condition.

In addition, optimization for polymeric insulators is not conducted. Therefore, there is no unifying vision on corona ring optimization for different voltages and insulators. In [25], the potential and electric field distribution were obtained for polymeric insulator at 345 kV. The effects of towers and bundled conductors were considered. However, the results are valid only for the dry condition and for the specific voltage of 345 kV. The effects of corona rings on the distributions was not considered. In [25], the electric field distribution was computed for polymeric insulators at voltages up to 1200 kV AC. In addition, in [25], corona rings and bundled conductors were modeled, and their effects on the electric field distribution were examined. However, potential distribution, which is important in flashover occurrence, under different conditions was not calculated, and the effect of towers, which can make significant differences in results, was not modeled. Likewise, it is vital to compute the electric field and potential distributions on the ceramic insulators to obtain a more comprehensive vision. In [28], the potential and the electric field distributions were obtained for a ceramic disc insulator at 330 kV by considering the effects of the tower and bundled conductors. However, corona rings and polymeric insulators as well as other voltages and different conditions were ignored.

In [29], potential and electric fields in ceramic insulators at 400 kV were studied by using the FEM method. The effect of corona rings on electric field distributions was obtained. The effects of towers and bundled conductors on the results are not addressed.

In this paper, both the ceramic cap and pin insulator and the polymeric insulator are used for calculating electric field and voltage distributions along at three different voltages: 230 kV, 400 kV, and 765 kV. The calculations are conducted in both dry and wet conditions. The comparisons are also presented between the two insulators in terms of voltages, corona ring size effectiveness, and bundled conductors. These features are significant in the design, selection, and performance of insulators [25] under specific conditions and provide comparative data in different systems, which enables designers to choose between ceramic and polymeric insulators by considering special conditions.

2. Simulation Models

At different voltage ratings of 230 kV, 400 kV and 765 kV, the creepage distance and the arc distance for both polymeric and ceramic insulators are different. Therefore, it is necessary for calculations to be done for three ceramic cap and pin insulators and three polymeric insulators at different voltages. The geometry of a polymeric insulator and a ceramic cap and pin were modeled in AutoCAD is shown in Figure 1. Since the tower may primarily affect the results and overall conclusions [32,33] for each system voltage, each systems' tower is modeled. The towers were involved in the calculations, and to decrease the time of the calculations, the effect of conductors of other phases is not considered.

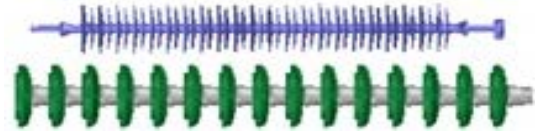


Figure 1. Models of the polymeric insulator and the ceramic cap and pin insulator, which were modeled in the AutoCAD for FEM computations

2.1. Models of Insulators, Towers and Corona Rings

Polymeric insulators are made out of a fiberglass rod to endure mechanical loads and a polymeric material housing consisting of the sheath and weathershed [24]. They are equipped with a metal fitting at both ground end and line end [24]. The detailed geometry of a polymeric insulator is shown in Figure 2a.

Ceramic disc insulators are made out of a number of cap and pin pieces so that by connecting a specific number of these pieces, a string is made. A detailed geometry of this kind of insulator, which is modeled for calculations of this study, is shown in Figure 2b.

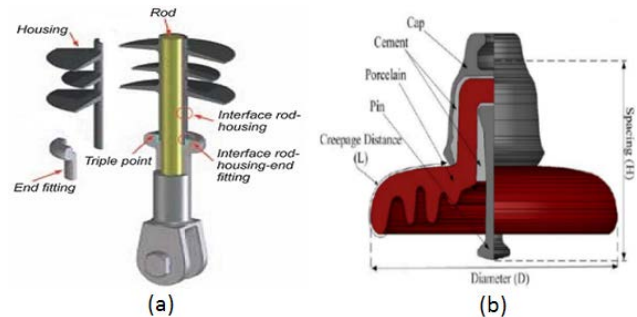


Figure 2. Detailed parts of a polymeric insulator and a piece of disc string, which the simulations and different strings are based on. a) Polymeric insulator detailed geometry. b) Cap and pin detailed geometry [34] in this study are $D=280$ mm, $H=170$ mm, and $L=380$ mm for all three system voltages

Table 1. Dimensions of polymeric insulator at different voltages

Voltage Rating (kV)	Creepage Distance (mm)	Dry Arc Distance (mm)
230	5815	2000
400	9525	3280
765	6600	5000

Table 2. Ring diameters of C-Type corona rings at different voltages for both insulators

Voltage Rating (kV)	Diameter in ground end (mm)	Diameter in line end (mm)
230	No Need	200
400	200	400
765	400	400

Table 3. Dimensions of ceramic cap and pin insulator at different voltages

Voltage Rating (kV)	Number of Discs	Creepage Distance (mm)	Dry Arc Distance (mm)
230	15	5700	2550
400	25	9500	4250
765	47	17860	7990

The dimensions of insulators' discs were extracted from the Iran Insulator Company (IIC) catalog [35], and dimensions of corona rings were recommended by the manufacturers [36,37]. The dimensions are noted in Table 1, Table 2, and Table 3. The corona rings, must be placed in the line end, in the ground end, or in both ends to decrease the electric field and voltage distribution along the string. For simulations, the installation height is set to 100 mm from the HV and/or ground end and the diameter of the ring tube is set to 45 mm. Corona rings are divided into two types of circular shapes: C-type and Racket types (R-type). In this paper, only the C-type is studied. The C-type corona rings, which are placed on both sides of insulators, are shown in Figure 3.

The dimensions of towers for each voltage rating are extracted from the Tavanir Electric Power Industry Co. catalog [38]. Based on these tower dimensions which are shown in Figure 4, simulated models of towers were built in AutoCAD, and then by transferring the models to a FEM software package, computations were conducted. A simulated half model of the tower is shown in Figure 4(d).

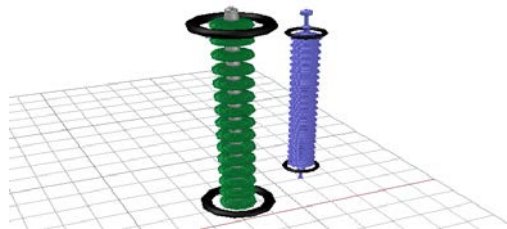


Figure 3. Schematic of a typical ceramic cap and pin and polymeric insulator with corona rings at both the line end and ground end and modeled in AutoCAD for FEM computations

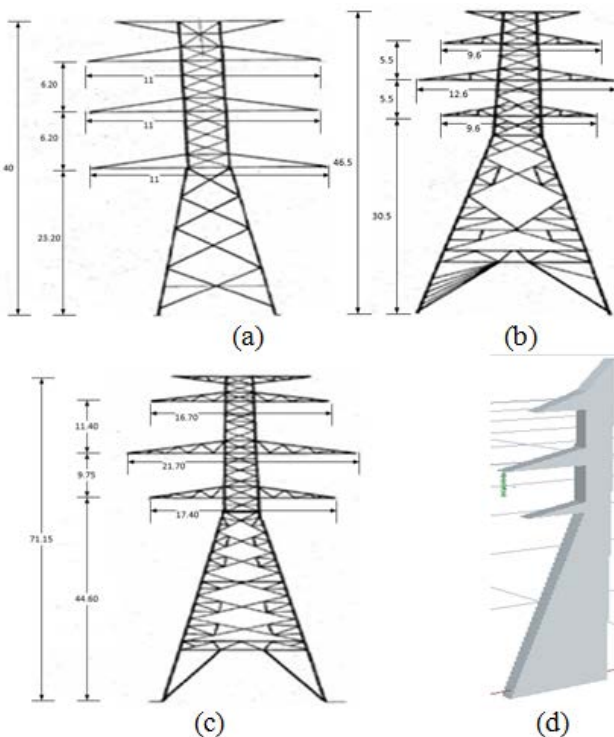


Figure 4. The towers with their dimensions (units are in meters) are used for three system voltages to model simulated towers for FEM computations. a) 230 kV tower dimensions. b) 400 kV tower dimensions. c) 765 kV tower dimensions. [38]. (d) Typical half model tower modeled in AutoCAD.

Table 4. Peak voltage of each phase for boundary condition

Rating Voltage (kV)	Peak Voltage in each Phase (kV)
230	188
400	462
765	625

2.2. Numerical Analysis Method

As the frequency of power line transmissions is low-50 Hz or 60 Hz - the problem of computing electric field and potential can be solved in a quasi-static state [39]. Therefore, by using the Laplace equation and inserting boundary conditions, the problem will be solved.

$$\nabla^2(V) = 0 \tag{1}$$

$$V_{\infty} = V_{\text{Earth}} = V_{\text{Tower}} = 0 \tag{2}$$

$$V_{\text{Line}} = (V/\sqrt{3}) \times \sqrt{2} \text{ (in each system voltage)} \tag{3}$$

After solving the potential equation, the distribution of the electric field can be obtained from equation (4):

$$E = -\nabla(V). \tag{4}$$

As mentioned in previous sections, all of the equations are solved by the FEM. The boundary conditions in the software are set to the following:

- Voltage on the conductors and the fitting ends of insulators is in accordance to Table 4.
- Voltage on towers, ground, and fittings at the line side of insulators is 0 V.
- Conductors and other parts without voltage are considered as float voltages with a total charge of 0 C.

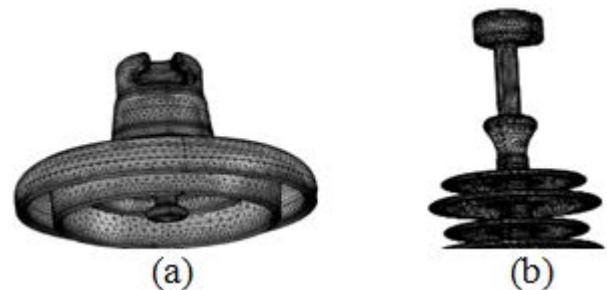


Figure 5. a) Meshed model of a disc of ceramic cap and pin insulator. b) Meshed model of a part of a polymeric insulator.

In the software package, after creating the geometry, each insulator, tower, and element must be divided into small boundaries for meshing. After meshing, the problem can be solved. In significant parts, the mesh was made smaller for more accurate results. As the number of meshes increases, the results become more accurate, but calculation time increases. Thus, a compromise must be made between calculation time and accuracy of results. For this reason, in the software, the number of meshes was set higher in insulators, corona rings, and bundled conductors than for other parts of the whole geometry. The number of meshes in insulators differed from 323,652 to 510,364. Schematics of meshed models for parts of insulators are shown in Figure 5.

In wet conditions, water droplets were simulated on insulators, and then the problem was meshed again and solved. The diameter of droplets was set to 5 mm with a

90 degree contact angle with the surface. The distance between droplets is considered to be 10 mm from each other. After adding the droplets for simulating wet condition, the number of meshes and calculation time increased significantly. Thus, another compromise was needed to decrease the time of simulation while preserving the accuracy. The relative permittivity of fiberglass, steel, silicone rubber, and water were considered to be 5, 1, 4, and 80, respectively.

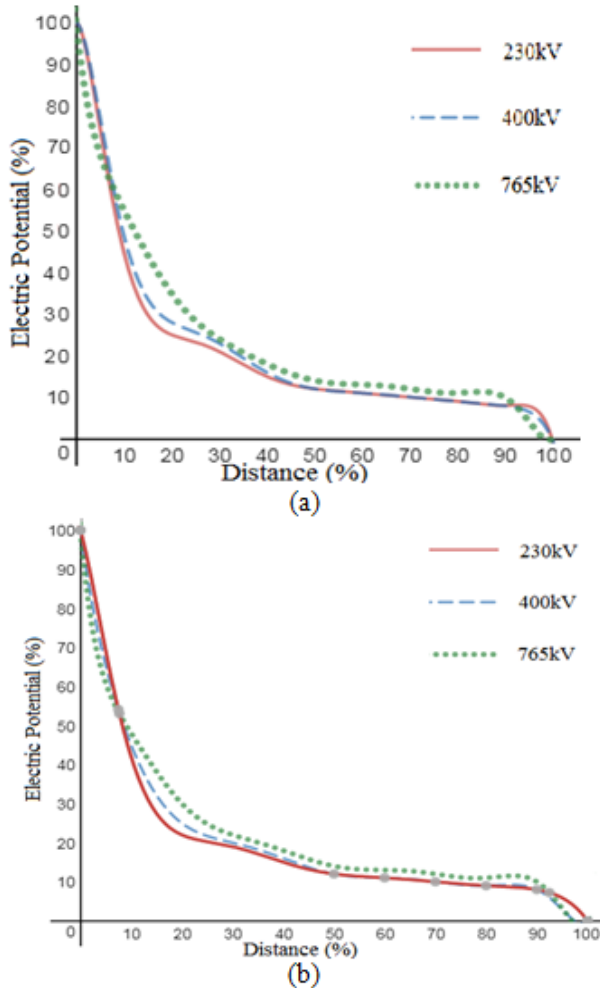


Figure 6. Voltage distribution for polymeric insulators along the insulation distance at the center line of the rods. The voltage is normalized against the maximum value for each voltage and distance is normalized against the insulation distance from the HV end to the ground end. a) Without corona ring. b) With corona ring

3. FEM Analysis

3.1. Potential Distribution

The potential distribution was calculated for both types of insulators with and without a corona ring for each of three different system voltages. The insulators were assumed to be clean. Based on Figure 6 and Figure 7, the voltage distribution for a polymeric and a disc insulator at voltages of 230 kV, 400 kV, and 765 kV are comparable. As the voltage distribution of a middle-phase is greater than the side-phases [28], these measurements were calculated for the middle phase of the system. The results show that the decrease/increase rate for two ends of the

curves for both disc and polymeric insulators is more than the middle. The voltage characteristic of the disc insulators is more even than the polymeric insulators, because polymeric insulators have fewer fittings and are three-piece constructions.

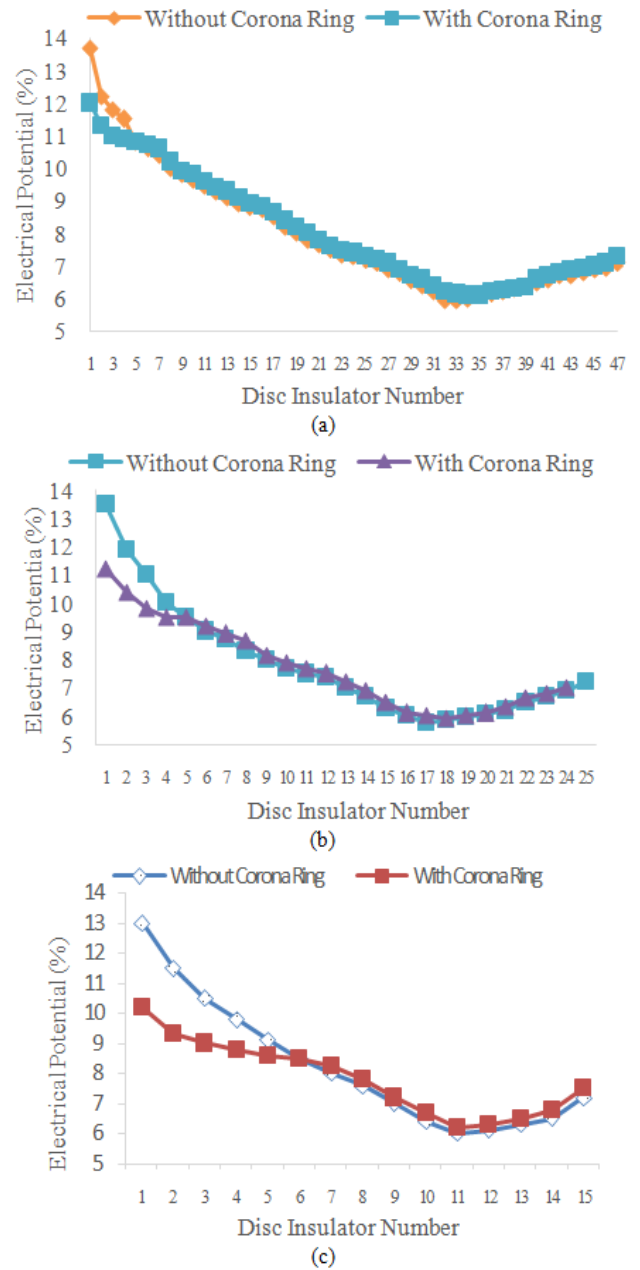


Figure 7. Voltage distribution on the discs of ceramic cap and pin insulators at different voltages. Disc numbers increase from the HV end to ground end. a) 765 kV disc insulator with 47 discs. b) 400 kV disc insulator with 25 discs. c) 230 kV disc insulator with 15 discs

It is clear, in the absence of a corona ring the bottom parts of the insulators, which are near the HV end, endure more voltage than when in the presence of a corona ring. Therefore, the presence of corona rings, can delayed aging of insulators. This inequality of voltage with the presence of a corona ring in disc insulators can be expressed by the string efficiency (SE) parameter:

$$SE = \frac{\text{Conductor Voltage}}{n \times \text{the voltage across the disc nearest to the conductor}}$$

In the above definition, n is number of discs in the ceramic cap and pin insulators. By considering string efficiency, it is clear that by adding the corona ring, this parameter will improve in insulators, which is desirable. In Table 5, SE is calculated for the first 4 discs of ceramic cap and pin insulators.

Table 5. String efficiency in ceramic cap and pin insulators, with and without the corona ring, for the first 4 discs by numbering from HV end to ground end. a) 230 kV. b) 400 kV. c) 765 kV

Disc Number	Without Corona Ring (%)	With Corona Ring (%)
1	51.28	65.36
2	57.97	71.68
3	63.49	74.07
4	68.03	75.76

Disc Number	Without Corona Ring (%)	With Corona Ring (%)
1	29.63	35.71
2	33.61	38.46
3	36.36	40.82
4	40	42.11

Disc Number	Without Corona Ring (%)	With Corona Ring (%)
1	15.53	17.73
2	17.44	18.83
3	18.03	19.34
4	18.50	19.52

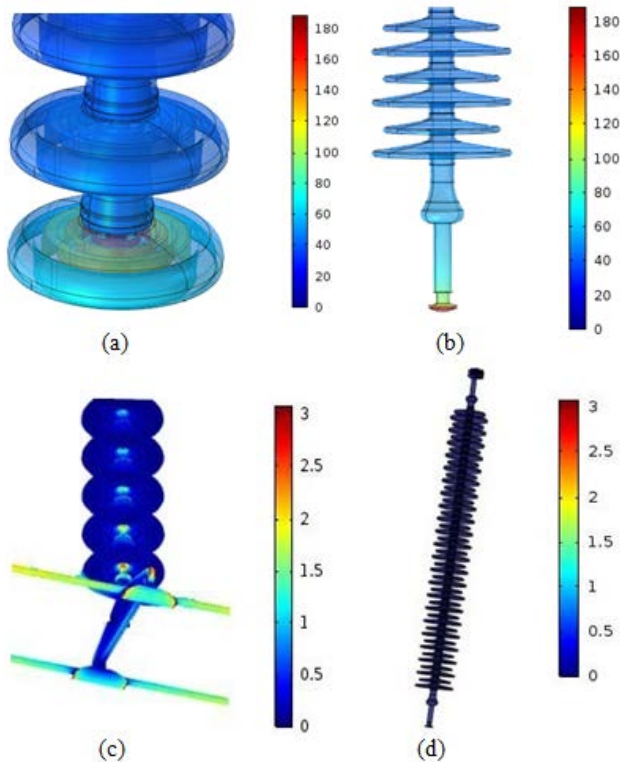


Figure 8. An example of 3D voltage (kV) and electric field (kV/cm) distribution on insulators with a 230 kV voltage. a) Voltage distribution along the ceramic cap and pin insulator. b) Voltage distribution along Polymeric insulator. c) Electric field distribution along the cap and pin insulator with 2 bundled conductors. d) Electric field distribution along the polymeric insulator

Table 6. The maximum electric field for different voltages with and without corona ring for polymeric insulators under dry condition. Corona threshold is 15 kV/cm.

Voltage Rating (kV)	Maximum E-field (kV/cm)		Decrease Percent of Maximum E-field (%)
	Without Corona Ring	With Corona Ring	
230	15.7	7.48	52.36
400	21.68	8.16	62.36
765	35.14	9.49	72.91

Table 7. The maximum electric field in different voltages with and without corona rings for ceramic cap and pin insulators under dry condition. The corona threshold is 15 kV/cm

Voltage Rating (kV)	Maximum E-field (kV/cm)		Decrease Percent of Maximum E-field (%)
	Without Corona Ring	With Corona Ring	
230	21.68	3.57	83.53
400	35.52	4.78	86.54
765	66.49	6.91	89.61

Table 8. The maximum electric field with corona ring under dry condition by considering bundled conductors for polymeric and ceramic cap and pin insulators. a) 230 kV. b) 400 kV. c) 765 kV

Number of bundled conductors	Maximum Electric Field (kV/cm)	
	Polymeric Insulator	Ceramic Insulator
2	4.18	2.27
4	3.94	2.03
6	3.43	1.72

Number of bundled conductors	Maximum Electric Field (kV/cm)	
	Polymeric Insulator	Ceramic Insulator
2	5.19	3.31
4	4.46	2.59
6	3.74	2.23

Number of bundled conductors	Maximum Electric Field (kV/cm)	
	Polymeric Insulator	Ceramic Insulator
2	6.80	5.37
4	5.54	4.28
6	4.62	3.55

3.2. Electric Field Calculations under Dry Condition

The electric field is calculated for both insulators at different system voltages by assuming they are all clean. 3D voltage and electric field distribution on the insulators with the voltage of 230 kV is shown in Figure 8. It is clear that the electric field increases as the voltage is increasing, and the maximum electric field occurs near the HV side. For the safety of insulators against corona, the maximum electric field in each voltage system must be under the corona occurrence threshold, which is considered in this study to be 15 kV/cm [40] in dry and clean weather. As shown in Table 6 and Table 7, in the three system voltages without the corona ring, all of them are above the threshold. After adding corona rings, we observe remarkable mitigation in the measurements of the maximum electric field for both insulator types. The percent decrease in the maximum electric field for the polymeric insulator at

voltages of 230 kV, 400 kV, and 765 kV is 52.36%, 62.36%, and 72.91%, respectively. For the ceramic insulator at voltages of 230 kV, 400 kV, and 765 kV it is 83.53%, 86.54%, and 89.61%, respectively. By considering the presence of towers in calculations it can be inferred from the electric field distribution with and without corona ring, that for all voltages above 230 kV both types of insulators need corona rings in order to decrease maximum electric field so that it is under the corona threshold. For voltages under 230 kV, each case must be considered separately for weather to add a corona ring or not.

Table 9. The maximum electric field at different voltages with and without corona rings for polymeric insulators under wet condition. Corona threshold is 8 kV/cm.

Voltage Rating (kV)	Maximum E-field (kV/cm)		Decrease Percent of Maximum E-field (%)
	Without Corona Ring	With Corona Ring	
230	22.14	10.32	53.39
400	32.09	11.67	63.63
765	51.10	14.15	72.30

Table 10. The maximum electric field at different voltages with and without corona rings for ceramic cap and pin insulators under wet condition. Corona threshold is 8 kV/cm.

Voltage Rating (kV)	Maximum E-field (kV/cm)		Decrease Percent of Maximum E-field (%)
	Without Corona Ring	With Corona Ring	
230	30.57	5.28	82.73
400	51.21	7.22	85.90
765	99.07	9.61	90.30

3.3. Calculations of Bundled Conductors

It is common in high voltage transmission lines to use bundled conductors. By adding multiple conductors instead of one, current magnitude decreases along with the electric field on conductors' surface, thereby reducing the corona. In each voltage rating, reliability increases by using bundled conductors, but in some voltages, economic conditions may restrict usage. It is clear that the number of conductors depends on the system voltage. In this study, when considering 2, 4, and 6 conductors per bundle, the distance between conductors is considered to be 50 cm. In Table 8, the trend of changing the maximum electric field based on the number of bundled conductors is shown for both insulator types. The effects of towers and corona ring are considered. It is clear in the Tables that increasing the number of conductors in each bundle decreases the maximum electric field.

3.4. Electric Field Calculations under Wet Condition

Presence of water droplets on the surface of insulators causes a high concentration of electric field intensity in some points, which leads to an increase in the maximum electric field in the insulators. On the other hand, in wet conditions, the electric field required for onset streamer propagation is considered to be 4.5-11 kV/cm [25,41-44], which is well below the threshold of the dry condition. The hydrophobic feature of the silicone rubber material in polymeric insulators also intensifies the electric field in

those insulators. In this study, the streamer threshold under the wet condition is considered to be 8 kV/cm, and it was assumed that water droplets are pure H₂O. In Table 9 and Table 10, the maximum electric field for the insulators are shown by considering effects of towers and corona rings based on voltage ratings. It is clear, for the three voltage ratings the maximum electric field has increased between 40 to 60 percent compared to the dry condition. Under the wet condition, the maximum electric field for the polymeric and the ceramic insulators for all voltages at 765 kV is above the threshold. Hence, it is necessary for these insulators to be able to resist corona discharge.

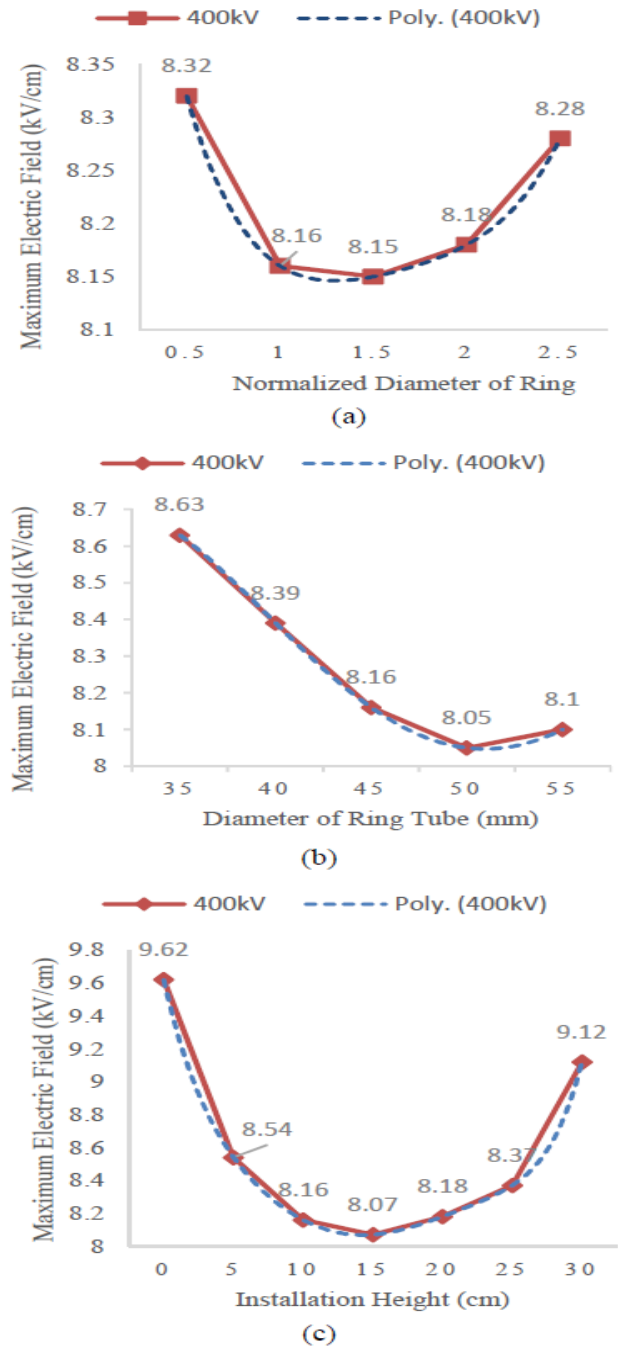


Figure 9. Maximum E-field variations of the polymeric insulator at 400 kV by changing parameters of the corona ring. Based on several points, the functions were interpolated in polynomial by chasing the trend of changes the optimum values extracted. a) Max. E-field against normalized ring diameter. It is normalized against the Table 2 values. b) Max. E-field against the diameter of the ring tube. c) Max. E-field against the installation height

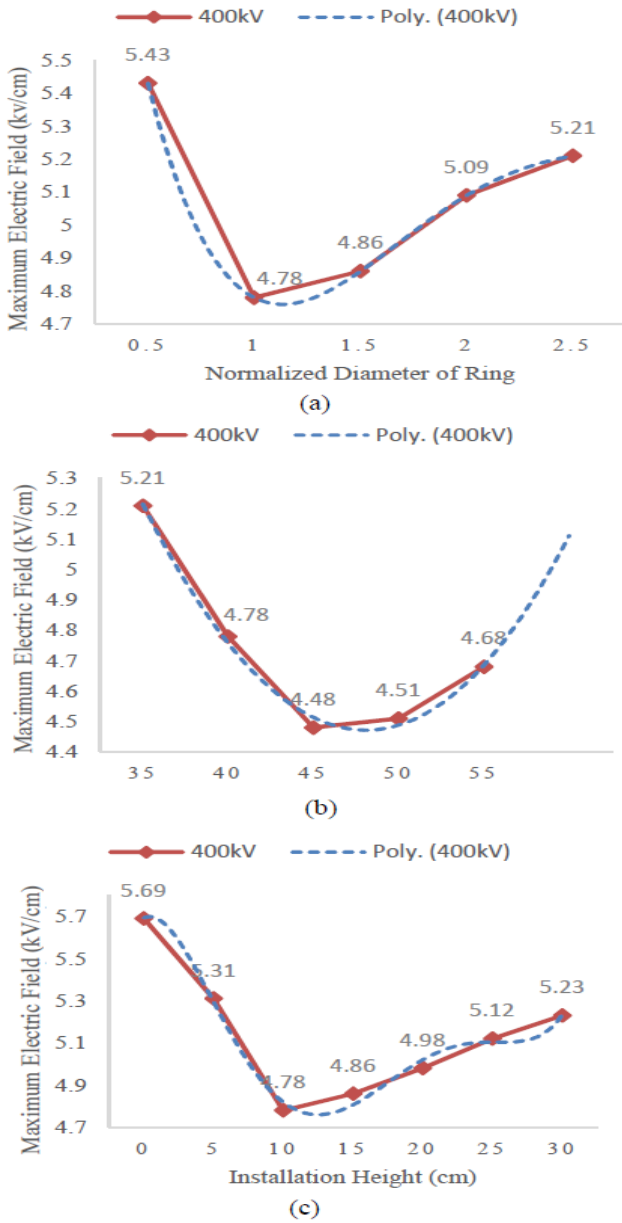


Figure 10. Maximum E-field variations of the ceramic cap and pin insulator at 400 kV by changing parameters of corona ring. Based on several points, the functions were interpolated in polynomial by chasing the trend of changes the optimum values extracted. a) Max. E-field against normalized ring diameter– it is normalized against the Table 2 values. b) Max. E-field against diameter of the ring tube. c) Max. E-field against installation height

Table 11. Optimum values of corona ring parameters in each voltage. a) Polymeric insulators. b) Ceramic insulators.

(a)

Voltage Rating (kV)	Ring Diameter (mm)		Diameter of Ring Tube (mm)	Installation Height (cm)
	ground end	Line end		
230	NoNeed	235	46	16
400	246	492	50	14
765	262	524	52	12

(b)

Voltage Rating (kV)	Ring Diameter (mm)		Diameter of Ring Tube (mm)	Installation Height (cm)
	ground end	line end		
230	NoNeed	232	44	15
400	238	476	48	13
765	252	608	53	11

4. Corona Rings Optimization

As shown previously, corona rings have a significant influence on the electric field distribution and in decreasing the maximum electric field, which leads to a reduction in the corona level under the suitable threshold. The presence of corona rings directly affects the reduction of losses due to corona and enhances productivity. Table 2, on which previous calculations were based, shows typical rings that are produced and recommended by manufacturers but are neither optimal nor the most efficient. In this part, for each insulator at different voltages, the parameters that affect corona rings are studied, and the maximum electric field is calculated by changing each parameter. Next, the optimal corona ring is extracted from the graphs. The important parameters are the diameter of the ring, the thickness (diameter of the ring tube), and distance from the end-fitting high voltage end or the ground end which is the installation height. Figure 9 and Figure 10 show the variations of the maximum electric field at 400kV, based on changing each parameter while considering the other two to be constant. In Figure 9, the diameter of the ring is scaled by amounts from Table 2 and changes in the parameter calculations were based on the information in Table 2. For example, for 400 kV insulators, two corona rings are considered on both sides, but for 230 kV only one is considered on the HV side. As the pattern of graphs is similar for other voltages they are not included in the paper, but the final result of optimum corona ring for each one is included. To obtain the optimum values, interpolated functions were used based on computations of the maximum electric field values in each state at different voltages. The optimum values are shown in Table 11. It is clear that for each voltage in polymeric and ceramic insulators, the optimum corona ring is different, and the effect of each parameter on changing the maximum electric field values is not the same for all.

5. Conclusion

Potential and electric field values are very important for designing and choosing equipment in transmission lines and substations. Therefore, two types of insulators – the polymeric and the ceramic – are compared under different conditions and voltages, enabling designers and manufacturers to have a more vivid picture for their work. In this study, potential and electric field calculations were made for the two types of insulators under dry and wet conditions for three different voltage ratings using the finite element method. Each type has specific features with both advantages and disadvantages.

Potential distribution values in the ceramic cap and pin insulators are nearer to each other than in the polymeric insulators; ceramic insulators endure lower electric field intensity in the presence of corona ring. Under the wet condition the calculations are more complicated. Polymeric insulators at 230 kV, 400 kV, and 765 kV, and ceramic insulators at 765 kV must be able to endure corona discharges because the maximum E-field exceeds the threshold. Optimizing the corona rings for each insulator type at each voltage showed that the parameters

of corona rings can significantly affect the maximum E-field. This might be useful for designing special corona rings for insulators, under special conditions, case by case.

References

- [1] Wang, H., Cheng, L., Liao, R., Zhang, S., Yang, L.: "Non-destructive testing method of micro-debonding defects in composite insulation based on high power ultrasonic", *High Voltage*, 4, (3), pp. 167-172, 2019.
- [2] Pernebayeva, D., Irmanova, A., Sadykova, D., Bagheri, M., James, A.: "High voltage outdoor insulator surface condition evaluation using aerial insulator images". *High Voltage*, 4, (3), pp. 178-185, 2019.
- [3] Yang, S., Jia, Z., Ouyang, X.: "Effects of algae contamination on the hydrophobicity of high-voltage composite insulators". *High Voltage*, 4, (3), pp. 234-240, 2019.
- [4] Sun, P., Sima, W., Jiang, X., Zhang, D., He, J., Ye, L.: "Review of accumulative failure of winding insulation subjected to repetitive impulse voltages". *High Voltage*, 4, (1), pp. 1-11, 2019.
- [5] Qi, B., Jiao, Y., Gao, C., Zhang, S., Zhao, X., Li, C.: "Influence of moisture on the interface charge of oil-pressboard composite insulation under DC voltage". *High Voltage*, 3, (1), pp. 73-77, 2018.
- [6] Yang, Z., Jiang, X., Han, X., Zhang, Z., Hu, J.: "Influence of pollution chemical components on AC flashover performance of various types of insulators". *High Voltage*, 2019.
- [7] Ojha, S.K., Purkait, P., Chatterjee, B., Chakravorti, S.: "Application of Cole-Cole model to transformer oil-paper insulation considering distributed dielectric relaxation". *High Voltage*, 4, (1), pp. 72-79, 2019.
- [8] Gao, Y., Liang, X., Bao, W., Wu, C., Li, S.: "Failure analysis of a field brittle fracture composite insulator: characterisation by X-ray photoelectron spectroscopy analysis". *High Voltage*, 2018.
- [9] Nazir, M.T., Phung, B.T., Yu, S., Zhang, Y., Li, S.: "Tracking, erosion and thermal distribution of micro-AlN-SiO₂ co-filled silicone rubber for high-voltage outdoor insulation". *High Voltage*, 3, (4), pp. 289-294, 2018.
- [10] M.S. Sanjari Nia, P. Shamsi, M. Ferdowsi, "Investigation of Various Transformer Technologies for HF Isolation Applications," *IEEE Transactions on Plasma Science*, pp. 1-1, 2020.
- [11] M.S. Sanjari Nia, S. Saadatmand, M. Altimania, P. Shamsi and M. Ferdowsi, "Analysis of Various Transformer Structures for High Frequency Isolation Applications", 2019 North American Power Symposium (NAPS), 2019.
- [12] M.S. Sanjari Nia, S. Saadatmand, M. Altimania, P. Shamsi, and M. Ferdowsi, "Analysis of Skin Effect in High Frequency Isolation Transformers", 2019 North American Power Symposium (NAPS), 2019.
- [13] M.S. Sanjari Nia, M. Altimania, P. Shamsi, and M. Ferdowsi, "Electric Field and Parasitic Capacitance Analysis for HF Transformers with Coaxial Winding Arrangements," *2020 IEEE Kansas Power and Energy Conference (KPEC)*, 2020.
- [14] M.S. Sanjari Nia, M. Altimania, P. Shamsi, and M. Ferdowsi, "Magnetic Field Analysis for HF Transformers with Coaxial Winding Arrangements," *2020 IEEE Kansas Power and Energy Conference (KPEC)*, 2020.
- [15] M. Altimania, M.S. Sanjari Nia, M. Ferdowsi, and P. Shamsi, "Analysis and Modeling of Non-Isolated Two-Phase Interleaved Boost Converter with Diodes-Capacitors Cells in the DCM", 2019 North American Power Symposium (NAPS), 2019.
- [16] M. Altimania, M.S. Sanjari Nia, M. Ferdowsi and P. Shamsi, "A new Topology of a High-Voltage-Gain DC-DC Converter Based on Modified Greinacher Voltage Multiplier," *2020 IEEE Kansas Power and Energy Conference (KPEC)*, 2020.
- [17] M. Altimania, M.S. Sanjari Nia, M. Ferdowsi and P. Shamsi, "A Non-Isolated High-Voltage-Gain DC-DC Converter with Modified Greinacher Voltage Multiplier in DCM," *2020 IEEE Kansas Power and Energy Conference (KPEC)*, 2020.
- [18] S. D. Nazemi, K. Mahani, A. Ghofrani, B.E. Kose, M. Amini, M. Jafari, 2019, "Techno-economic analysis and optimization of a microgrid considering demand-side management", Published in Arxiv, arXiv preprint arXiv:1908.06352.
- [19] A. Ghofrani, S. D. Nazemi, M. Jafari, "Prediction of building indoor temperature response in variable air volume systems", *Journal of Building Performance Simulation* 13 (1), 34-47, 2019.
- [20] A. Ghofrani, S. D. Nazemi, M. Jafari, 2019, "HVAC load synchronization in smart building communities", *Sustainable Cities and Society*, 2019, 101741.
- [21] J. Faiz and A. Ghasemi, "A new method for estimation of losses in inverter-fed induction machines including electrical insulation losses," *2016 IEEE International Power Electronics and Motion Control Conference (PEMC)*, 2016.
- [22] S. Yazdani, M. Ferdowsi, and P. Shamsi, "Internal Model Based Smooth Transition of a Three-Phase Inverter Between Islanded and Grid-Connected Modes," *IEEE Transactions on Energy Conversion*, pp. 1-1, 2019.
- [23] S. Yazdani, M. Ferdowsi, M. Davari, and P. Shamsi, "Advanced Current-Limiting and Power-Sharing Control in a PV-Based Grid-Forming Inverter under Unbalanced Grid Conditions," *IEEE Journal of Emerging and Selected Topics in Power Electronics*, pp. 1-1, 2019.
- [24] Kluss, J., Chalaki, M.R., Whittington, W., Rhee, H., Whittington, S., Yadollahi, A.: "Porcelain insulation – defining the underlying mechanism of failure" *High Voltage*, 2019.
- [25] Doshi, T., Gorur, R., Hunt, J.: "Electric field computation of composite line insulators up to 1200 kV AC" *IEEE Transactions on Dielectrics and Electrical Insulation*, 18, (3), pp. 861-867, 2011.
- [26] Mishra, D., Dutta, S., Baral, A., Haque, N., Chakravorti, S.: "Use of Interfacial Charge for Diagnosis and Activation Energy Prediction of Oil-Paper Insulation Used in Power Transformer". *IEEE Transactions on Power Delivery*, 34, (4), pp. 1332-1340, 2019.
- [27] Tuttelberg, K., Loper, M., Kilter, J.: "Correcting Systematic Errors in Corona Losses Measured With Phasor Measurement Units". *IEEE Transactions on Power Delivery*, 34, (6), pp. 2275-2277, 2019.
- [28] Huang, D., Ruan, J., Cai, W., Li, T., Wei, Y., Liu, J.: "Flashover prevention on high-altitude HVAC transmission line insulator strings". *IEEE Transactions on Dielectrics and Electrical Insulation*, 16, (1), pp. 88-98, 2009.
- [29] Mhamdi, B., Tegar, M., Mekhaldi, A.: "Potential and electric field distributions on HV insulators string used in the 400 kV novel transmission line in Algeria" *2013 IEEE International Conference on Solid Dielectrics (ICSD)*, 2013.
- [30] Zhang, B., He, J., Cui, X., Han, S., Zou, J.: "Electric field calculation for HV insulators on the head of transmission tower by coupling CSM with BEM" *IEEE Transactions on Magnetics*, 42, (4), pp. 543-546, 2006.
- [31] Sebestyn, I.: "Electric-field calculation for HV insulators using domain-decomposition method" *IEEE Transactions on Magnetics*, 38, (2), pp. 1213-1216, 2002.
- [32] Reddy, B.S., Verma, A.R.: "Novel technique for electric stress reduction across ceramic disc insulators used in UHV AC and DC transmission systems" *Applied Energy*, 185, pp. 1724-1731, 2017.
- [33] Zhang, B., Cui, Y., Zhang, W., et al.: "Voltage and electric field distribution along porcelain long rod insulator string in AC 500kV transmission line". *2016 IEEE International Conference on High Voltage Engineering and Application (ICHVE)*, 2016.
- [34] Akbari, E., Mirzaie, M., Rahimnejad, A., Asadpoor, M.B.: "Finite Element Analysis of Disc Insulator Type and Corona Ring Effect on Electric Field Distribution over 230-kV Insulator Strings". *International Journal of Engineering & Technology*, 1, (4), p. 407, 2012.
- [35] Iran Insulator Co. catalog, Tehran, Iran, pp. 6-12 [online]. Available: <http://iraninsulator.ir/portfolio-grid-2-col-mini/>, 2017.
- [36] Xinjiang New Energy Catalog, China, 2009.
- [37] Phillips, A., Kuffel, J., Baker, A., et al.: "Electric Fields on AC Composite Transmission Line Insulators". *IEEE Transactions on Power Delivery*, 23, (2), pp. 823-830, 2008.
- [38] Tavanir Electric power industry Company catalog, Iran, 2003.
- [39] Liu, S., Sheng, C., Meng, F., et al.: "Electric field disturbance caused by an unmanned aerial vehicle flying near the HV power transmission line" *2016 IEEE International Conference on High Voltage Engineering and Application (ICHVE)*, 2016.
- [40] Looms, J.: "Insulators for high voltages [Books and Reports]". *IEEE Power Engineering Review*, 11, (6), p. 45, 1991.

- [41] Rizk, F.A.: "Mechanism of insulator flashover under artificial rain". *Proceedings of the Institution of Electrical Engineers*, 122, (4), p. 449, 1975.
- [42] M. Farhadi and M. Abapour, "Three-Switch Three-Phase Inverter With Improved DC Voltage Utilization," *IEEE Transactions on Industrial Electronics*, vol. 66, no. 1, pp. 14-24, 2019.
- [43] M. Farhadi, M. T. Fard, M. Abapour, and M. T. Hagh, "DC-AC Converter-Fed Induction Motor Drive With Fault-Tolerant Capability Under Open- and Short-Circuit Switch Failures," *IEEE Transactions on Power Electronics*, vol. 33, no. 2, pp. 1609-1621, 2018.
- [44] M. Farhadi, M. Abapour, and B. Mohammadi-Ivatloo, "Reliability analysis of component-level redundant topologies for solid-state fault current limiter," *International Journal of Electronics*, vol. 105, no. 4, pp. 541-558, 2017.



© The Author(s) 2020. This article is an open access article distributed under the terms and conditions of the Creative Commons Attribution (CC BY) license (<http://creativecommons.org/licenses/by/4.0/>).